Research Article

Influence of cooling rate on the ferrite content and microstructures in CD3MWCuN castings

Longlong Liao[1] · Scott Chumbley[1]

Abstract

Highly alloyed CD3MWCuN was chosen to investigate the influence of cooling rates on the ferrite content of duplex stainless steels. It is known that cooling rate can influence the overall ferrite/austenite ratio, and achieving the proper balance of phases is crucial in producing a casting with suitable mechanical and corrosion properties. Initial experiments were carried out to study the ferrite/austenite ratio as a function of cooling involved samples obtained using different cooling rates through the solidification temperature as well as different cooling rates from the homogenization temperature. A single keel bar was obtained, sectioned, and recast at six different solidification cooling rates. Each of the six castings was then sectioned into six pieces and each piece cooled from the homogenization temperature to produce six different homogenization cooling rates. Backscattered electron imaging was used to measure the phase percentages and observe the microstructures. The ferrite content was found to increase with increasing homogenization cooling rates. It was also found that the homogenization cooling rate should be higher than 200 °C/h in order to get high ferrite contents (> 40%). As the cooling rate slows, intermetallic phases such as sigma start to precipitate at the grain boundaries.

Keywords Duplex stainless steels · Ferrite content · Point-count · BSE-SEM

1 Introduction

Duplex stainless steels (DSSs), which consist of a 50/50 mixture of austenite (γ) and ferrite (α), are extensively used in a variety of applications including marine, oil, pulp and petrochemical industries due to their excellent mechanical properties and corrosion resistance [1–3]. The physical properties of DSS are between those of ferritic stainless and austenitic stainless steels but more likely to be closer to carbon steel [4]. In comparison with pure austenitic grades, DSS have better stress corrosion, pitting, and crevice corrosion resistance [3].

The ferrite content plays a crucial role in the corrosion and stress corrosion cracking resistance of DSS [4]. Research has also found that the ferrite content is related to low temperature toughness of DSS welds [5]. Much research has been done to investigate the effect of the various alloying elements on the ferrite content [6, 7]. However, less work has been conducted on investigating the effect of cooling rates on the ferrite content. It has long been known that cooling rate in the solid state from high temperature in steels affects both the room temperature phase distribution and the microstructure, as evidenced by the formation of metastable phases such as martensite and the variation in lamellar spacing that can be produced in pearlite. What is less known is how cooling rate can affect the ferrite/austenite ratio seen in duplex stainless steels. This is of particular importance in large steel castings, where changes in section thickness can produce a variety of starting microstructures before homogenization heat treatments, and result in different cooling rates from that homogenization temperature. Thus, estimation of the ferrite/austenite ratio is important.

✉ Longlong Liao, longlongliao@gmail.com | [1]Department of Material Science and Engineering, Iowa State University, Hoover Hall 2220, Ames, IA 50010, USA.

Determination of the ferrite/austenite ratio is complicated by the fact that intermetallic phase formation has been noted in highly alloyed steels when cooling at the slower rates from the homogenization temperature [8]. While the amounts that have been seen are relatively small, usually less than five volume percent, they produce a significant drop in the fracture toughness of DSS [8] and can affect what would have been the expected ferrite/austenite ratio. Intermetallics usually are seen to form at the expense of the ferrite phase, so measurements made on the basis of magnetic means can be affected.

Historically, the ferrite content of steels has been estimated using constitution diagrams such as those determined by Schaeffler [9], DeLong [10] and the Welding Research Council (WRC-92) [11]. These constitution diagrams are all based on the determination of Cr and Ni alloying addition equivalents; they do not include cooling rates and do not accurately predict the ferrite content when the Cr content is extremely high, as is the case for highly alloyed stainless steels such as CD3MWCuN. Thus, a need exists for a more study of the ferrite/austenite ratio for highly alloyed steels, one that includes the effect of cooling rate as well as composition variation.

In this paper, the effect of cooling rate on the ferrite content was investigated. Results obtained in material of a single composition that had been solidified and cooled at various rates, then homogenized and cooled again at various rates will be presented.

2 Experimental procedure

Keel bars $35 \times 20 \times 180$ mm in size of CD3MCuN were received for examination. The nominal composition of the as-received bars is shown in Table 1. A single keel bar was selected (Fig. 1a) and sectioned into six pieces of roughly equal weight. From these pieces of assumed identical composition, six cylindrical samples (18 mm diameter $\times$ 30 mm length) were produced by remelting and controlled cooling casting (Fig. 1b). The six samples were heated to 1525 °C under an Argon atmosphere, held for 30 min, and then cooled to 400 °C with six different solidification rates (10, 20, 50, 100, 200, 300 °C/h), after which the furnace was powered off and the samples were allowed to cool to room temperature. This range of cooling rates was selected based upon industry input. Computer models have shown that rates various can be produced in extremely large castings. The desire was to account for rates that might be expected if such castings cooled using normal conditions and in cases where the cooling procedure may either fail or be disrupted in the process.

Eight slices approximately 2.5 mm thick were cut from each of the six solidified cylindrical samples. One slice from each of the six different solidification rates was then selected, and the chosen slices were encapsulated under an Ar atmosphere for subsequent controlled cooling from the homogenization temperature (Fig. 1c). This was repeated five more times, producing a total of six

Table 1 Nominal composition of received CD3MWCuN material (major elements)

Element	Mn	Si	Ni	Cr	Mo	Fe	Cu	W	N
wt%	0.42	0.73	7.37	24.74	3.69	61.3	0.677	0.54	0.23

Fig. 1 **a** Keel bar selected for the experiment. **b** Example of a recast sample solidified at a controlled rate. **c** Typical encapsulated samples for controlled cooling from the homogenization temperature

encapsulations, each containing one slice from each of the six solidification rate samples. Each capsule of six slices was then heated homogenized. A homogenization heat treatment of 1250 °C for 4 h was used in this study. This decision was based on the work of Dupont [12], who found complete dissolution of the sigma phase and homogenization of Mo only happened after a heat treatment of 1205 °C for 4 h. This same study also found that this heat treatment produces corrosion resistance of CN3MN and CK3MCuN cast alloys on the level of their wrought counterpart alloys [12]. Thus, by using an even higher temperature than suggested by Dupont, it was assumed any differences seen in phase formation between samples cooled at similar rates could only be due to residual differences in the initial microstructure produced by the selected solidification rates.

Once homogenized, the six capsules were cooled from the homogenization temperature at six different rates (10, 20, 50, 100, 200, 300 °C/h) to 400 °C, after which the furnace was powered off and they were allowed to air cool to room temperature. The remaining two additional slices from the different solidification samples were homogenized then water quenched and air-cooled from the homogenization T. This produced a total matrix of 48 different samples, all ostensibly with the same composition and homogenization, varying only in solidification rate and cooling rate from the homogenization temperature, as shown in Fig. 1.

All samples were ground and polished with 180–600 grit papers followed by 6 and 1 µm suspended diamond slurry solution. The ferrite content of the samples was checked by backscattered electron (BSE) imaging using a JEOL 6060LV scanning electron microscope (SEM). A manual method was used where BSE images obtained using the SEM were examined and phase percentages determined using a superimposed grid. The manual method was chosen over an automated system since the complexity of the microstructure in many cases was such that judgments often had to be made as to what phase was actually being counted. The different phases distinguished using BSE-SEM were designated as being either ferrite, austenite, or intermetallic. This was done to speed identification and because the different intermetallics that can form are often difficult to distinguish using only BSE-SEM imaging [13]. From a practical standpoint, all the intermetallics that form in duplex steels result in degradation of the mechanical and corrosion properties and should be avoided.

Ten images were obtained from each sample to measure ferrite content. In the example shown in Fig. 2, the darker area is ferrite, the gray is austenite, and the white is intermetallic, which is primarily sigma phase. A 29 × 21 grid was placed on each image examined. Points on the test grid that fell within the microstructural feature of interest
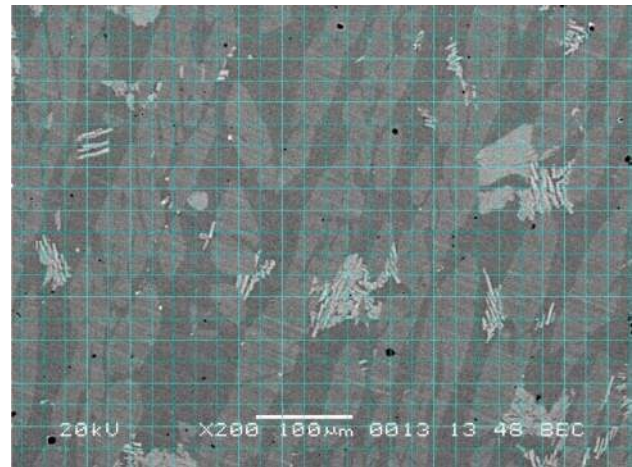

Fig. 2 Example image showing a superimposed test grid used for the manual method

counted as one point for that phase; points falling on the feature boundaries counted as half a point for each phase.

The results obtained optically were also compared to values obtained using magnetic measurements. Samples were examined using a Fisher Feritscope FMP30, where five measurements were taken on the same polished samples used for microscopy observations. In general, the measured values corresponded reasonably well with the optical measurements, typically being with ±10% of the microscopy values, except in cases when ferrite content is low (less than 10%). Since the Feritscope only had the ability to measure ferrite percentage, all values reported in this study were obtained using quantitative microscopy.

3 Results

3.1 Microstructure

Figure 3 shows a series of pictures for one solidification rate, namely the sample cooled at 200 °C/h from the molten state, as an example of the types of images obtained during the course of this study. Eight different images are shown, covering the cooling from the homogenization temperature at rates of 10, 20, 50, 100, 200, 300 °C/h, water quench and air cool as is shown in the matrix displayed in Fig. 3. As can be seen from the pictures, intermetallic phases tend to precipitate as the homogenization cooling rates decreases. At the slowest cooling rates (10, 20, 50 °C/h), the ferrite appears to be almost entirely consumed by intermetallic formation. The scale of the intermetallic structure makes it difficult to tell if there is any ferrite remaining between the intermetallic laths. Not until the cooling rate increases to 100 °C/h is there an
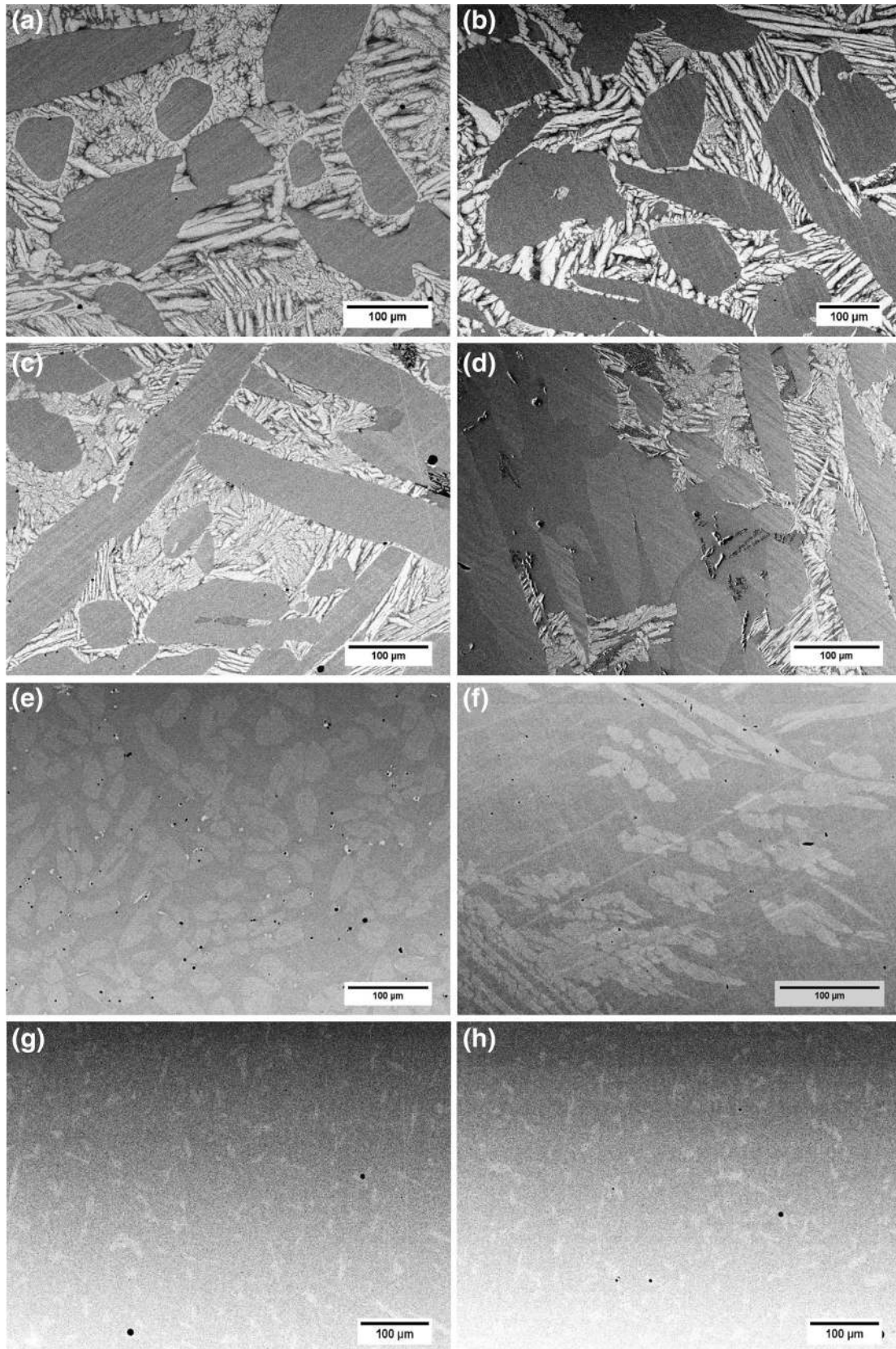
Fig. 3 200 °C/h solidification rate and **a** 10 °C/h homogenization cooling rate, **b** 20 °C/h, **c** 50 °C/h, **d** 100 °C/h, **e** 200 °C/h, **f** 300 °C/h, **g** air cool, **h** water quench

appreciable amount of ferrite retained. The cooling rate of 200 °C/h (Fig. 3e) is the point where primarily two phases ($\alpha + \gamma$) are seen with the amount of intermetallic phase (small white areas) present falling to < 5 vol%, an acceptable level where mechanical properties are not adversely affected. As cooling rate increases to 300 °C/h, no intermetallic phase was found. For the water quenched and air cool samples, the structures were primarily ferrite (matrix) with only small amounts of austenite formed (≤ 2%).

3.2 X-ray diffraction

X-ray diffraction (XRD) was used to determine the major type of intermetallic forming. Studies were carried out on samples cooled from the solidification temperature at a rate of 200 °C/h, as it was assumed that these results would be applicable to the entire range of samples. This assumption was based on the fact that the microstructures observed in the 200 °C/h solidification rate set of samples contained all of the phases present in the remaining samples and therefore were representative of all the samples, except for the relative amounts present. The results obtained are shown in Fig. 4.

When using XRD phase percentages of less than five percent are often difficult to detect, especially in Fe-based systems. It is clear by simple observation of Fig. 3a–c that the 200 °C/h solidification set has significant intermetallic phases present at the lower homogenization cooling rates and this is mirrored in the XRD data of Fig. 4a–c. The 10 °C/h, 20 °C/h and 50 °C/h samples have large peaks that can be identified as belonging to the sigma phase apart from those peaks associated with ferrite and austenite. This is especially true when compared to the higher rate samples. Studies have suggested that the initial intermetallic that forms in highly alloyed steels is chi, quickly changing to the more stable sigma phase in a relative short period of time [14]. It would seem that the slower cooling rates allow this change to occur. From a mechanical properties and corrosion standpoint, both sigma and chi are detrimental, lowering fracture strength and pulling Cr and Mo from the matrix. Both chi and sigma grow at the expense of ferrite [15].

3.3 Quantitative measurements

Table 2 shows the ferrite, austenite and intermetallic percentage obtained. The uncertainty associated with the measurements is ± 4%. As seen in the BSE-SEM images (Fig. 3), the matrix is changing from being almost all ferrite at the highest cooling rates to a mixture of ferrite plus austenite at the intermediate rates, with the amount of intermetallic starting to increase substantially once the

cooling rate from the homogenization temperature drops below 200 °C/h.

Figures 5, 6 and 7 show the phase content results in both two-dimensional and three-dimensional plots. A clear trend of ferrite content increasing with increasing rate of cooling from the homogenization temperature is shown (Fig. 5). Cooling rate through the solidification temperature appears to have a slight effect on ferrite content, again with the higher cooling rates producing a higher amount of ferrite in the final structure, although this effect is weak and quicky lost as homogenization cooling rate decreases.

Intermetallic content increases as the cooling rate from the homogenization temperature slows (Fig. 6). As intermetallic formation primarily occurs via nucleation and growth in the ferrite, this is not surprising since you would expect intermetallic to rise as ferrite content falls.

Austenite content remains relatively consistent even though there are variations across the entire sample space (Fig. 7). Slight drops are seen at the very high cooling rates (where ferrite was seen to be favored) and at the intermediate cooling rate from homogenization of ≈ 100 °C/h.

4 Discussion

4.1 Solidification rate

Figure 8 shows the Fe–Cr–Ni pseudo-binary diagram at 60% Fe section. According to the diagram, the solidification order for CD3MWCuN is $L \rightarrow \delta + L \rightarrow \delta \rightarrow \delta + \gamma \rightarrow \gamma + \delta + \sigma$. It is known that solidification cooling rates and alloy composition have a profound effect on the microstructure and ferrite content of stainless steels [16], and that the microstructure can range from a duplex structure of ferrite and austenite to fully austenitic or ferritic for a wide variety of stainless steels depending on cooling rates. It is also known that sigma phase formation can occur at slower solidification cooling rates [17].

The ferrite content after solidification was not measured in this paper since the cast alloy studied is always homogenized before use. This is necessary to completely dissolve any sigma phase that may have formed upon cooling and to produce homogenization of the Mo, which can be difficult [12].

The residual effect of solidification rate can be deduced by observation of Figs. 5, 6 and 7. At any given cooling rate from the homogenization temperature, a faster solidification rate will promote a higher percentage of ferrite in the casting. The effect is fairly slight, probably due to the effectiveness of the homogenization process. At the higher initial solidification rates where more ferrite is expected to be
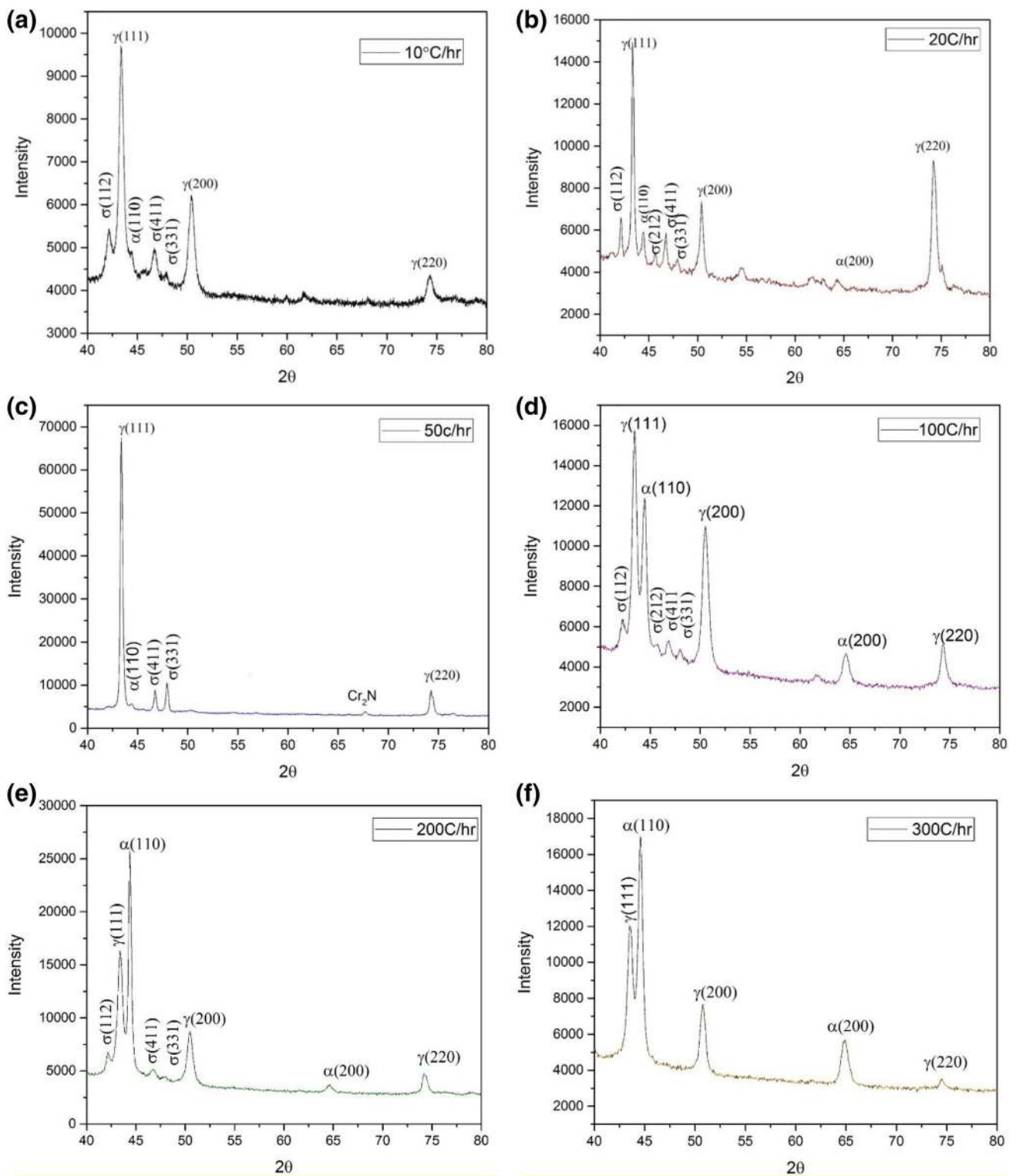
Fig. 4 XRD Results of second trial 200 °C/h solidification rate with six different homogenization rate **a** 10 °C/h, **b** 20 °C/h, **c** 50 °C/h, **d** 100 °C/h, **e** 200 °C/h and **f** 300 °C/h

retained, the slowest cooling rate from the homogenization temperature can result in an overall increase in the amount of intermetallic observed in the final conditions.

If the initial casting had been cooled more slowly to give a higher initial austenite percentage, there would be less ferrite to decompose into intermetallic + austenite. Evidence

Table 2 Ferrite percentage (%) of CD3MWCuN (ferrite: δ, austenite: γ, intermetallic: *I*)

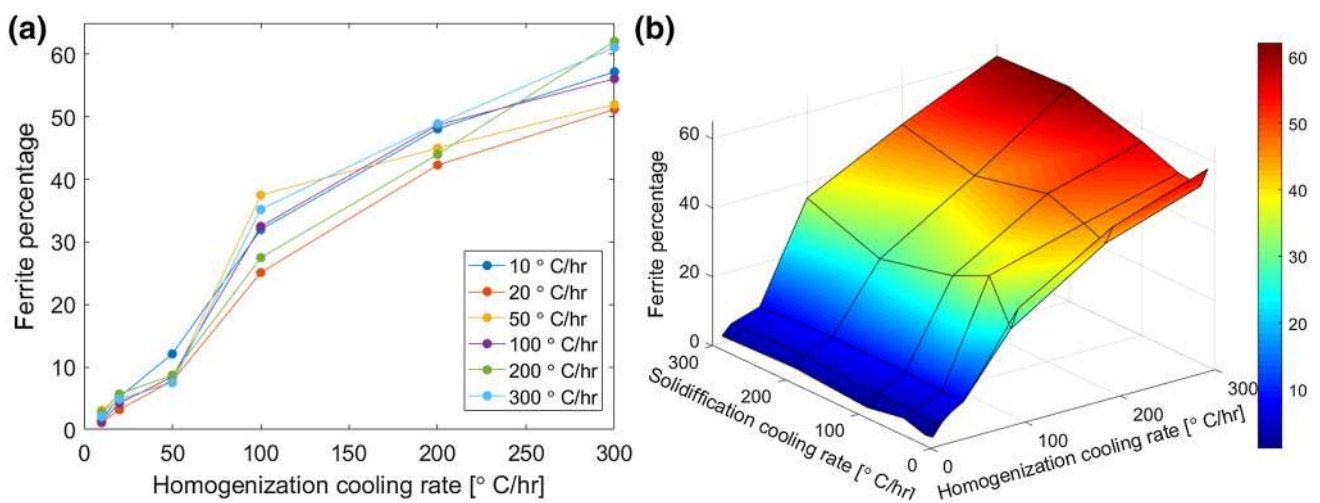| Homogeniza- tion cooling rate	Solidification cooling rate (°C/h)																	
	10 °C/h			20 °C/h			50 °C/h			100 °C/h			200 °C/h			300 °C/h		
	δ	γ	*I*	δ	γ	*I*	δ	γ	*I*	δ	γ	*I*	δ	γ	*I*	δ	γ	*I*
10 °C/h	1.5	56.4	42.1	1.1	51.6	47.3	3.1	49.9	47	1.2	51.7	47.1	2.8	35.2	62	2.1	39.9	58
20 °C/h	5.2	55.6	39.2	3.2	51.7	45.1	4.5	51.5	44	4.2	50.6	45.2	5.7	55.2	39.1	4.9	53.1	42
50 °C/h	12.1	49.7	38.2	7.8	52.1	40.1	7.8	47.2	45	8.5	53.4	38.1	8.7	51.8	39.5	7.5	53.5	39
100 °C/h	32	43.7	24.3	25.1	49.8	25.1	37.5	42.2	20.3	32.5	45.4	22.1	27.5	51.3	21.2	35.2	46.5	18.3
200 °C/h	48.1	51	0.9	42.3	57.1	0.6	45	54.3	0.7	48.7	50.2	1.1	44	55.2	0.8	48.9	50.2	0.9
300 °C/h	57.2	42.5	0.3	51.2	48.4	0.4	52	47.5	0.5	56.1	43.7	0.2	62.1	37.9	0	61.1	38.4	0.5
Water quench	97.8	2.2	0	98.5	1.5	0	98.1	1.9	0	98.5	1.5	0	98.0	2.0	0	98.7	1.3	0
Air cool	98.1	1.9	0	98.3	1.7	0	98.8	1.2	0	98.2	1.8	0	97.8	2.2	0	99.2	0.8	0

Fig. 5 **a** Two-dimensional and **b** three-dimensional plots of ferrite content as a result of solidification rate and cooling from the homogenization temperature
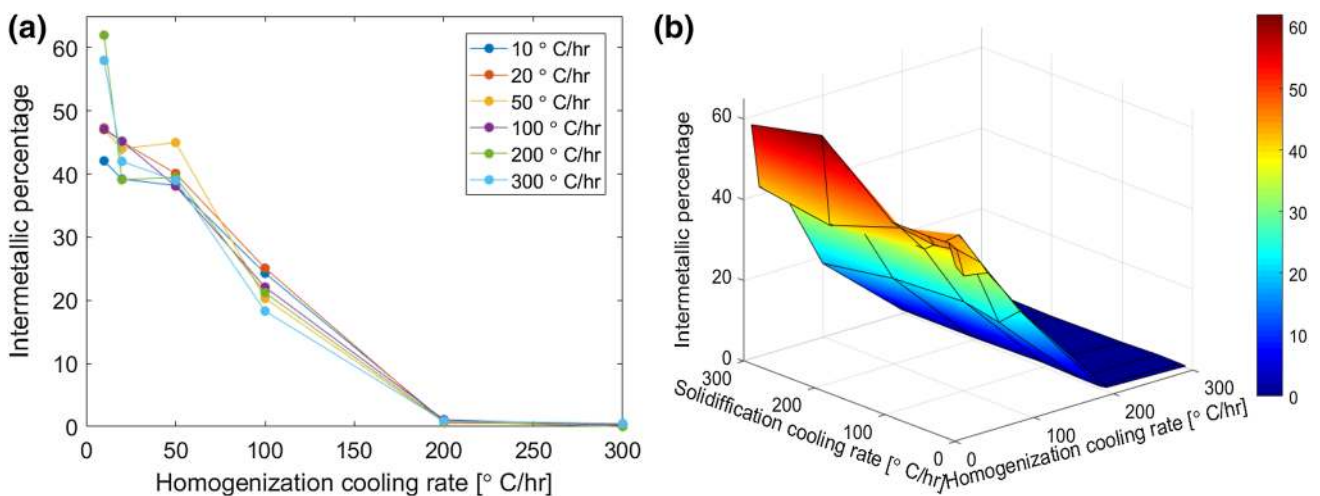

Fig. 6 **a** Two-dimensional and **b** three-dimensional plots of intermetallic content as a result of solidification rate and cooling from the homogenization temperature
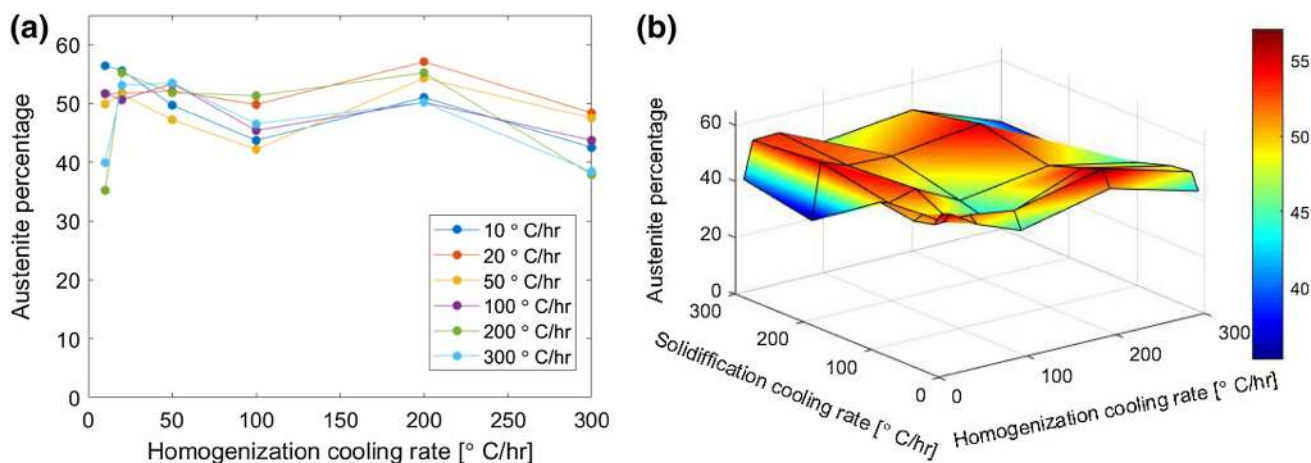
Fig. 7 **a** Two-dimensional and **b** three-dimensional plots of austenite content as a result of solidification rate and cooling rate from the homogenization temperature
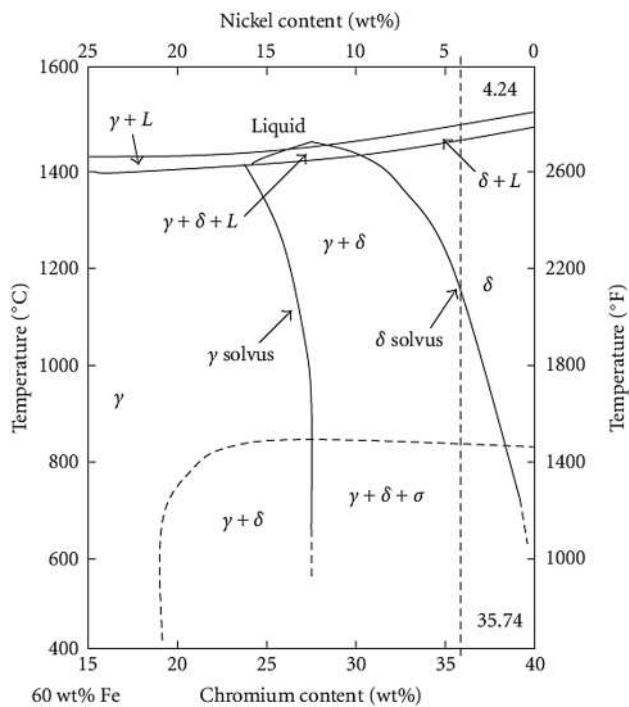

Fig. 8 Fe–Cr–Ni pseudo-binary diagram at 60% Fe [17]

of this is shown in Fig. 6 for the 200 °C/h and 300 °C/h solidification rate samples which have the highest intermetallic present after the slowest cooling rate.

4.2 Cooling from the homogenization temperature

In the water quenched and air-cooled samples, the structure is almost 100% ferrite, as confirmed by microstructure analysis and magnetic measurements using a Feritscope. At the highest cooling rates, the desired 50/50 mixture for

this alloy composition is slightly ferrite rich, ranging up to 60% ferrite at the highest rate of 300 °C/h. Measurements show there is less than 1.2% of sigma phase found in the alloy at the highest cooling rates (200 °C/h and 300 °C/h), regardless of how much was present initially due to a slow solidification rate, attesting to the efficiency of the high temperature, long time homogenization treatment.

SEM-BSE images reveal that at slower cooling rates intermetallic formation occurs at the expense of ferrite. This is in agreement with studies that show cooling rates from the homogenization temperature can result in inter-metallic formation occurring in duplex and superaustenitic steels after relatively short times, primarily on the grain boundaries initially [18], greatly affecting the fracture toughness of castings [19]. Ferrite percentage becomes extremely low at the slowest cooling rates (Table 2) on the order of a few percent. These low amounts are consistent with Feritscope measurements also. At the lowest rates used in this study, thermodynamic equilibrium is more likely. Phase transformations for the four slowest cooling rates produce large scale intermetallic formation. In this paper, sigma phase is the primary intermetallic phase formed which is consistent with previous work [20].

At the intermediate cooling rates, the equilibrium amount of ferrite decreases and existing δ-ferrite is consumed, transforming to intermetallics + new austenite. This should result in an overall slight increase in the amount of austenite. It is somewhat surprising, then, to see a slight dip in austenite percent at intermediate cooling rates (50–100 °C), on the order of 5 vol%. Given that the error in measurements is estimated to be ±4 vol%, it is possible that this dip is primarily due to measurement uncertainty. However, it is also possible that at these lower cooling rates, the alloy spends a significant amount of time at lower temperatures where the phase diagram is extremely

complex [21, 22]. At this time, it is impossible to determine the exact cause for this dip by examining the data of this study.

At the highest rates (greater than 200 °C/h), the ferrite/austenite balance is determined by the CCT and TTT curves [13, 14, 23] Starting from an entirely (δ) ferritic structure as cooling rate slows the δ-ferrite > austenite transformation occurs, resulting in a decrease in the amount of ferrite and formation of austenite in accordance with the TTT curve. At these cooling rates, the ferrite percentage is higher than 40%, which is a typical number for duplex stainless steels [24]. The ferrite percentage ranges from 42 to 49% for the 200 °C/h homogenization cooling rate and from 50 to 60% at the higher 300 °C/h rate.

5 Conclusion

From the results of this study, we can draw the following conclusions:

1. The homogenization heat treatment used, based on the recommendation of Dupont (12) did an excellent job at producing an homogenous structure. When homogenized in this manner less than 4% differences were seen in the ferrite/austenite ratio, regardless of cooling rate through the solidification temperature.
2. The ferrite content in CD3MWCuN increases as the rate of cooling from the homogenization temperature increases.
3. Cooling CD3MWCuN from the homogenization temperature should be higher than 200 °C/h in order to avoid extensive intermetallic formation and maintain the ferrite content.
4. Cooling rates slower than 200 °C/h will produce intermetallic phases in CD3MWCuN. The predominant intermetallic phase is sigma, and it forms at the expense of the ferrite phase. Significant amounts (20–50 vol%) will form at cooling rates slower than 100 °C/h.

Compliance with ethical standards

Conflict of interest The authors declare that they have no conflict of interest.

References

1. David SA, Witek JM, Hebble TL (1987) Effect of rapid solidification on stainless steel weld metal microstructures and its implications on the Schaeffler diagram. Weld Res 66:289-s–300-s
2. Philips NSL, Chumbley LS, Gleeson B (2009) Phase transformations in cast superaustenitic stainless steels. J Mater Eng Perform 18:1285–1293
3. Bugat S, Besson J, Gourgues AF, Guyrn F, Pineau A (2001) Microstructure and damage initiation in duplex stainless steel. Mater Sci Eng A 317:32–36
4. Lundin CD, Chou CPD (1983) Hot cracking susceptibility of austenitic stainless steel weld metals. WRC Bull 289:1–80
5. Lundin CD, Delong WT, Spond DF (1975) Ferrite-fissuring relationships in austenitic stainless steel metals. Weld Res 54(8):241–246s
6. Olson DL (1985) Prediction of austenite weld metal microstructure and properties. Weld J 64(10):281s–295s
7. Vitek JM, David JA (1986) The sigma transformation in austenitic stainless steels. Weld J 65(4):106s–111s
8. Wen S, Lundin CD, Baten G (2001) Metallurgical evaluation of cast duplex stainless steels and their weldments, Final report Vol. 1 submitted to US Department of Energy, Award Number—DE-FC36-00 ID13975
9. Schaeffler A (1949) Constitution diagram for stainless steel weld metal. Metal Prog 56:680
10. Delong WT (1974) Ferrite in austenitic weld metal. Weld J 53:273s–286s
11. Kotechi DJ, Siewert DTA (1992) WRC-92 constitution diagram for stainless steel weld metals: a modification of the WRC-1988 diagram. Weld J 71(5):171s–178s
12. Dupont J, Farren JD (2011) Influence of heat treatment time and temperature on the microstructure and corrosion resistance of cast superaustenitic stainless steels. Corrosion 67(5):055002-1–055002-11
13. Leber HJ, Niffenegger M, Tirbonod B (2001) Microstructural aspects of low cycle fatigued austenitic stainless tube and pipe steel. Mater Sci Eng A 314:32–36
14. Kim YJ, Ugurlu O, Jiang C, Gleeson B, Chumbley LS (2007) Microstructural evolution of secondary phases in the cast duplex stainless steels CD3MN and CD3MWCuN. Met Trans 38(2):203–211
15. Kim YJ, Chumbley LS, Gleeson B (2004) Determination of isothermal transformation diagrams for sigma-phase formation in cast duplex stainless steels. Met Trans 35A:3377–3386
16. Lippold JC, Savage WF (1979) Solidification of austenitic stainless steel weldments: part I-A proposed mechanism. Weld Res 59:362-s–374-s
17. Sieurin H, Sandstrom R (2007) Sigma phase precipitation in duplex stainless steel 2205. Mater Sci Eng A 444:271–276
18. Sieurin H, Sandstrom R, Westin EM (2006) Fracture toughness of the lean duplex stainless steel LDX 2101. Metall Mater Trans A 37A:2975–2981
19. Muller C, Chumbley LS (2009) Fracture toughness of heat treated superaustenitic stainless steels. J Mater Eng Perform 19(5):714–720
20. Reick W, Phol M, Padilha FA (1990) Three types of embrittle in ferritic–austenitic duplex stainless steels. Metal Int 3(8):46–50

21. Pohl M, Storz O, Glogowski T (2007) Effect of intermetallic precipitation on the properties of duplex stainless steel. Mater Charact 58(1):65–71
22. Muthupandi V, Srinivasan P, Seshadri SK, Sundaresan S (2003) Effect of weld metal chemistry and heat input on the structure and properties of duplex stainless steel welds. Mater Sci Eng A 358(1–2):9–16
23. Kim YJ, Chumbley LS, Gleeson B (2008) Continuous cooling transformation in cast duplex stainless steels CD3MN and CD3MWCuN. J Mater Eng Perform 17(2):224–239
24. Johnson E, Kim YJ, Chumbley LS, Gleeson B (2004) Initial phase transformation diagram determination for the CD3MN cast duplex stainless steel. Scr Mater 50(10):1351–1354